Dynamic Structure of a Protein Hydrogel: A Solid-State NMR Study

ARTICLE *in* MACROMOLECULES · NOVEMBER 2001

Impact Factor: 5.8 · DOI: 10.1021/ma010768j

Dynamic Structure of a Protein Hydrogel: A Solid-State NMR Study

S. B. Kennedy, E. R. deAzevedo,† W. A. Petka, and T. P. Russell

Department of Polymer Science and Engineering, University of Massachusetts, Amherst, Massachusetts 01003

D. A. Tirrell

Division of Chemistry and Chemical Engineering, 210-41, California Institute of Technology, Pasadena, Califronia 91125

M. Hong*

Department of Chemistry, Iowa State University, Ames, Iowa 50011

Received May 4, 2001

ABSTRACT: ^{13}C and ^{15}N solid-state NMR spectroscopy has been used to study the dynamic structure of a genetically engineered multidomain protein hydrogel that contains two leucine-zipper domains and a central polyelectrolyte domain. ^{13}C NMR spectra show that on the microsecond time scale the central domain is isotropically mobile while the leucine-zipper domains are rigid. This supports the hypothesis that the central domain acts as the flexible swelling agent of the gel network while the terminal domains form intermolecular aggregates. ^{13}C isotropic chemical shifts indicate that the terminal domains are helical, while the central domain has a random coil conformation. On the millisecond time scale, the leucine-zipper domains are highly dynamic, as determined from the ^{13}C-detected ^{15}N CODEX experiment. The motion is rigid-body in nature with a correlation time of about 80 ms at room temperature and has an average amplitude of about 50°. Several specific motional models are considered by comparing simulated and experimental exchange intensities as a function of the recoupling time for ^{15}N chemical shift anisotropy. The experimental data are consistent with two of the models considered: a random jump model and a uniaxial rotation model. The implications of this motion to strand exchange between helical bundles are discussed.

Introduction

Thermoreversible hydrogels are desirable materials because of their applications in drug delivery and tissue engineering.[1−4] Artificial protein hydrogels are particularly interesting because they afford the possibility of combining material properties with biological functionality.[5] To improve and ultimately control the macroscopic properties of thermoreversible hydrogels, a detailed understanding of the molecular structure and dynamics of the gel network is important.

A common characteristic of physical gels is the coexistence of rigid segments that associate to form interchain junction points and soft segments that allow swelling and prevent precipitation of the network from the solvent.[6−8] This feature has recently been suggested as the basis for gelation of a genetically engineered multidomain protein solution. This protein, designated as ACA here, contains two terminal domains made of heptad repeats following the leucine-zipper motif (Figure 1) that flank a central polyelectrolyte domain, $[(AG)_3PEG]_{10}$. It gels reversibly under suitable temperature and pH conditions.[5] The leucine-zipper motif, found in transcription factors and structural proteins, has a heptad periodicity commonly denoted abcdefg.[9,10] Hydrophobic amino acids occupy positions a and d, with position d being primarily leucine, while charged residues typically occupy positions e and g. Helix formation places the hydrophobic residues along one side of the helix, so that the favorable hydrophobic interaction promotes association of helices to form coiled coils or helical bundles. Stability of the associations is modulated by the charged residues at positions e and g under various pH conditions.[11]

MRGSHHHHHHGSDDDDKA
– helix – IGDHVAPRDTSYRDPMG
– [(AG)$_3$PEG]$_{10}$ – ARMPT
– helix – IGDHVAPRDTSW

helix = SGDLENE / VAQLERE / VRSLEDE / AAELEQK / VSRLKNE / IEDLKAE

Figure 1. Amino acid sequence of the protein used in this study. The two end domains are designated as "helix", and the central domain is a repetitive sequence rich in Ala, Gly, and Glu. Short amino acid sequences link the three domains. A His_6 tag is inserted in the amino terminus for protein purification by metal affinity chromatography.

Macroscopic physical properties of this genetically engineered protein hydrogel have been characterized by diffusing wave spectroscopy (DWS).[5] Here, the dynamic autocorrelation function of light scattered from sulfonated polystyrene (SPS) beads embedded in the gel network yielded the root-mean-squared displacement of the particles, $\langle r(t)^2 \rangle$. Results characteristic of a visco-

† Current address: Departamento de Fisica e Informatica, Instituto de Fisica de Sao Carlos, Universidade de Sao Paulo, Sao Carlos (SP), Brazil Caixa Postal 369, CEP:13560-970.

* To whom correspondence should be addressed: Tel 515-294-3521, Fax 515-294-0105, e-mail mhong@iastate.edu.

10.1021/ma010768j CCC: $20.00
Published on Web 11/07/2001

elastic gel were found between pH 8 and pH 9.5 at room temperature. On the basis of visual observation, DWS, and fluorescence experiments, it was proposed that gelation of the multidomain protein ACA occurs as a result of the balance between the oligomerization of the helical ends and the swelling of the central polyelectrolyte domain.[5] At low pH, acidic residues such as Glu are protonated, stabilizing all three domains. With no propensity to swell, the polypeptide chains aggregate and precipitate. Near neutral pH, the Glu residues become deprotonated and negatively charged, causing the Glu-rich central domain to swell while the helical bundles remain, thus forming a gel. At very high pH, the leucine zippers are destabilized by the high charges and dissociate to form a viscous solution.

DWS and fluorescence experiments require the use of bulky extrinsic probes to obtain information on the dynamics of the protein hydrogels. These extrinsic probes can potentially perturb the hydrogel network and do not yield direct information on the polypeptide chain dynamics. Solid-state nuclear magnetic resonance (NMR) spectroscopy, on the other hand, is a powerful noninvasive spectroscopic method that can directly examine the polypeptide chains comprising the gel network. Magic-angle spinning (MAS) solid-state NMR techniques can now be applied to both rigid solids and partially mobile solids to obtain information on the molecular structure and dynamics.[12,13] Here we report solid-state NMR evidence that supports the model of gelation proposed earlier for the ACA protein hydrogel. Our ^{13}C NMR results indicate differential dynamics between the central domain and the terminal domains of the protein on the sub-microsecond time scales. ^{15}N exchange NMR shows the presence of significant millisecond time scale motions in the leucine-zipper domains. We have determined the correlation time and amplitude of this slow motion and suggest a motional mechanism that accounts for the reversibility of gelation on the molecular level. These results represent the first NMR measurements of millisecond time scale dynamics in a large protein (22 kDa) with site resolution.

Experimental Section

Protein Expression and Purification. The multidomain protein ACA was prepared by expression of the corresponding artificial gene in an *Escherichia coli* host strain SG13009 containing the repressor plasmid pREP4 (Qiagen, Chatsworth, CA). Construction of the artificial gene in the expression plasmid PQE9 (Qiagen) has been previously reported.[5] This expression plasmid encodes an N-terminal hexahistidine sequence that affords protein purification by immobilized metal affinity chromatography. Cultures were grown at 37 °C in 2xYT (16 g of casein hydrolysate, 10 g of yeast extract, and 5 g of NaCl per liter of culture for 1 L cultures) media supplemented with ampicillin (100−200 mg/L). The cells were then sedimented by centrifugation at 22 000*g* for 10 min and resuspended in a M9 salt solution (60 g of Na_2HPO_4, 30 g of KH_2PO_4, 5 g of NaCl, and 10 g of NH_4Cl per liter). Sedimentation and resuspension of the cell pellet in fresh M9 salt solution were repeated three times to wash the cells of the initial 2xYT media. The cells were finally resuspended in a minimal media containing 60 g of Na_2HPO_4, 30 g of KH_2PO_4, 5 g of NaCl, 10 mg of $CaCl_2$, 120 mg of $MgSO_4$, and 1 mg of thiamine per liter and supplemented by unlabeled amino acids and labeled ^{15}N and ^{13}C sources as described below. When the cells grew to optical densities $OD_{600} > 2$, expression was induced by the addition of 1 mM isopropyl-β-thiogalactoside. After 4 h, cultured cells were sedimented by centrifugation at 22 000*g* for 10 min. The sedimented cells were resuspended in a sonication buffer (50 mM NaH_2PO_4, 300 mM NaCl, 10 mM imidazole, pH 8) and frozen at −20 °C. Cells were lysed by thawing and sonication, and the supernatant was collected for purification. The protein was purified by affinity chromatography on a nickel nitrilotriacetic acid resin (Ni^{2+}−NTA, Qiagen) following the native purification protocol provided by Qiagen.

Isotopic Labeling of Proteins. To obtain structural and dynamical constraints for multiple sites without losing spectral resolution, we labeled the protein ACA in ^{13}C selectively and extensively rather than uniformly or site-specifically.[14] The selective and extensive ^{13}C labeling was carried out by supplementing the M9 media with a combination of [2-^{13}C] glycerol (2 g/L) and 10 unlabeled amino acids Glu, Gln, Arg, Pro, Asp, Asn, Ile, Thr, Met, and Lys at 100 mg each per liter.[15] These 10 amino acids are all products of the citric acid cycle. Their addition to the M9 media inhibited their labeling, so that only amino acids synthesized from the glycolysis pathway and the pentose phosphate pathway (Gly, Ala, Val, Leu, Ser, Tyr, Trp, Phe, His, and Cys) were labeled. On the basis of the biosynthetic pathways, this [2-^{13}C] glycerol-based TEASE (10 amino acid selective and extensive) labeling protocol labels mainly backbone Cα sites and few side chain carbons.[15]

Two samples with slightly different ^{15}N-labeling schemes were used in our studies. In the first sample, ^{15}N-labeled ammonium chloride (1 g/L) was used as the only labeled nitrogen source in the growth medium. The yield for this sample was 15 mg per liter of culture. In the second sample, the ^{15}N-labeling level was improved by supplementing the minimal media with both ^{15}N-labeled Glu (100 mg/L), an important nitrogen precursor for many amino acids, and ^{15}N-labeled ammonium chloride. The amounts of the unlabeled citric acid cycle amino acids were reduced to 50 mg/L, and unlabeled Tyr, Trp, Phe, His, and Cys, which are not present in the protein sequence, were also added to the growth media to increase the protein yield. Gln was not added in the second synthesis, resulting in the partial labeling of Gln and Glu. The yield for this synthesis was 30 mg per liter of culture.

NMR Sample Preparation. The purified protein ACA was dialyzed against a large volume of distilled water and lyophilized. Dried powder was packed into a 4 mm NMR rotor and then hydrated with distilled water. The hydration content varied from 30% to 50% (w/w) for different samples. The rotor containing the sample was subject to several heating and cooling cycles to induce gel formation. These gels were more concentrated than those used in the DWS experiments, because further dilution caused the onset of large-amplitude motions that interfere with cross-polarization and significantly reduce the experimental sensitivities. The samples were kept at a constant humidity of 80% at 4 °C before the experiments.

NMR Spectroscopy. The NMR experiments were performed at a magnetic field of 7.0 T using a Bruker DSX-300 spectrometer (Billerica, MA). The spectrometer operates at 75.5 MHz for ^{13}C and 30.4 MHz for ^{15}N. A 4 mm $^{1}H/^{13}C/^{15}N$ triple-resonance MAS probe was used for all experiments. The spinning speed was regulated to ±2 Hz. The experiments were conducted between 293 ± 2 K (room temperature) and 308 ± 2 K. Proton decoupling fields of 105−125 kHz were applied, and the two-pulse phase modulation (TPPM) scheme was used during the acquisition time.[16] Typical ^{13}C and ^{15}N 90° pulse lengths were 4 and 5 μs, respectively. The contact time for $^{1}H-^{13}C$ cross-polarization was 300 μs.

The $^{15}N-^{13}C$ 2D correlation experiment for resonance assignment was conducted using a previously published pulse sequence that transfers the polarization between ^{15}N and ^{13}C by rotational echo double-resonance (REDOR) spectroscopy.[14,17,18] The 2D $^{13}C-^{13}C$ correlation spectrum was obtained using a standard ^{1}H-driven ^{13}C spin diffusion sequence. Frequency discrimination in the indirect dimension was achieved using the States method.[19] For the $^{15}N-^{13}C$ 2D spectrum, 224 scans were added for each t_1 point, and 36 t_1 points were collected for each of the cosine and sine data sets. The dwell time for the evolution period was 363.6 μs, which corresponded to two rotor periods for a spinning speed of 5.5 kHz. The maximum ^{15}N evolution time was 13 ms, correspond-

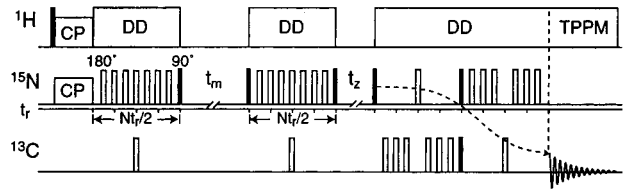

Figure 2. Pulse sequence for the ^{13}C-detected ^{15}N CODEX experiment. A train of rotor synchronized 180° pulses (open rectangles) on the ^{15}N channel before and after the mixing period t_m reintroduces the ^{15}N chemical shift anisotropy. Segmental reorientations during t_m interfere with the refocusing of the magnetization, thus reducing the ^{15}N magnetization. The ^{15}N magnetization is transferred to ^{13}C by a TEDOR sequence[27] and detected. Filled rectangles represent 90° pulses. DD = dipolar decoupling, CP = cross-polarization, and TPPM = two-pulse phase modulation.

ing to a ^{15}N resolution of 24 Hz. The ^{13}C−^{13}C correlation experiment used 32 scans per t_1 point and 180 t_1 points at an increment of 60.6 μs.

^{13}C-Detected ^{15}N CODEX Spectroscopy. Millisecond-time scale motions in the protein hydrogel were investigated using the ^{13}C-detected ^{15}N CODEX (centerband-only detection of exchange) technique,[20,21] which combines magic-angle spinning with exchange spectroscopy. The anisotropic ^{15}N chemical shift frequency is reintroduced under MAS by a train of 180° pulses spaced at half a rotor period, t_r, apart, for N rotor periods. The ^{15}N chemical shift is measured before and after a mixing period, t_m, during which reorientational motions occur (Figure 2). The changing molecular orientations alter the ^{15}N frequency, thus modulating the ^{15}N signal by the difference frequency $\cos(\Phi_1 - \Phi_2)$, where Φ_1 and Φ_2 are the time-averaged orientation-dependent frequencies before and after t_m, respectively. Since $\cos(\Phi_1 - \Phi_2) < 1$ for $\Phi_1 \neq \Phi_2$, reorientational motions reduce the ^{15}N signal intensities compared to a reference spectrum acquired without the mixing time. Thus, intensity differences between the exchange spectrum and the reference spectrum indicate the presence or absence of motion.

The ^{15}N chemical shift anisotropy, whose magnitude is represented by δ, is an excellent probe for molecular motions. First, ^{15}N−^{15}N dipolar couplings in proteins are relatively weak; thus, ^{15}N spin diffusion is inefficient within a mixing time of about 1 s. This leaves motion as the primary mechanism for exchange, thus simplifying the interpretation of CODEX spectra. Second, the magnitude and orientation of amide ^{15}N chemical shift tensors in proteins are well-known and are relatively uniform compared to ^{13}C chemical shift tensors.[22−27] This simplifies the determination of motional amplitudes from the CODEX spectra.

The CODEX-modulated ^{15}N signals were detected indirectly through ^{13}C by transferring the ^{15}N magnetization to neighboring ^{13}Cα sites using a transferred-echo double-resonance (TEDOR) sequence.[28] ^{13}C detection provides both higher resolution and sensitivity than ^{15}N, as discussed before.[29]

Information on the motional correlation times and amplitudes is extracted from the intensity difference between the exchange spectrum, $S(t_m,\delta Nt_r)$, and the reference spectrum, $S(0,\delta Nt_r)$.[21] The normalized pure-exchange signal

$$E(t_m,\delta Nt_r) = \frac{\Delta S}{S_0} = \frac{S(0,\delta Nt_r) - S(t_m,\delta Nt_r)}{S(0,\delta Nt_r)} \qquad (1)$$

results only from sites that have reoriented during t_m. Plotting $E(t_m,\delta Nt_r)$ as a function of t_m yields a decay curve whose decay constant corresponds to the correlation time, τ_c, of the motion. Alternatively, the pure-exchange intensity can be plotted as a function of the ^{15}N chemical shift recoupling time Nt_r. For $t_m \gg \tau_c$, small-amplitude motions require longer Nt_r to be detected by the ^{15}N chemical shift frequency, while large-amplitude motions require shorter Nt_r. Thus, the Nt_r dependence of the pure-exchange intensity provides information on the amplitude of the motion (see below). Normalizing the exchange spectrum $S(t_m,Nt_r)$ with the reference spectrum S_0 also removes the effects of T_1 and T_2 relaxation during the t_m and Nt_r periods.

The CODEX experiment was optimized first through a ^{15}N cross-polarization (CP)[30] experiment. Then a ^{13}C-detected test experiment with ^{1}H−^{15}N CP and ^{15}N−^{13}C TEDOR transfer was carried out. This test resembles the CODEX experiment except for the lack of a mixing period. The ^{13}C and ^{15}N pulse lengths and ^{1}H−^{15}N CP condition were optimized by maximizing the ^{13}C signals. An optimal ^{1}H−^{15}N CP contact time of 700 μs was found. To minimize the effects of long-term drifts of radio-frequency (rf) powers, the CODEX spectra for different mixing times and recoupling times were block-averaged, where each block consisted of interleaving reference and exchange experiments. The ^{15}N T_1 relaxation time of the protein hydrogel is longer than 7 s at 50% hydration. Thus, we reduced the signal-averaging time by using the same reference spectra for exchange experiments with t_m differing by less than 250 ms. Typically, 8192 scans were coadded for each exchange spectrum. Most CODEX spectra were acquired at a spinning speed of 5.5 kHz.

Simulations. The Nt_r-dependent CODEX intensities $E(t_m,\delta Nt_r)$ were simulated by weighting the CODEX subcurves $\epsilon(\beta_R,\delta Nt_r)$ for various reorientation angles, β_R, by the reorientation-angle distribution, $R(\beta_R,t_m)$,[31]

$$E(t_m,\delta Nt_r) = \frac{\Delta S}{S_0} = \int_{0°}^{90°} R(\beta_R,t_m)\,\epsilon(\beta_R,\delta Nt_r)\,\mathrm{d}\beta_R \qquad (2)$$

Equation 2 is strictly valid only for axially symmetric tensors, where a single reorientation angle, β_R, between the unique tensor axes before and after the motion is sufficient to describe the motion. For asymmetric tensors, three reorientation angles, α_R, β_R, and γ_R, must be considered. The amide ^{15}N chemical shift tensor in peptides has an asymmetry parameter (η) of about 0.2. Thus, β_R is the most important reorientation angle.

The subcurves, $\epsilon(\beta_R,\delta Nt_r)$, are calculated as the REDOR curves of the difference frequency between the rigid-limit tensors before and after the motion,

$$\epsilon(\beta_R,\delta Nt_r) = \langle 1 - \cos(N\int_0^{t_r/2}(\omega_2(t) - \omega_1(t))\,\mathrm{d}t)\rangle \qquad (3)$$

Here ω_1 and ω_2 are the orientation-dependent ^{15}N chemical shift frequencies before and after the motion. The angle brackets indicate powder averaging over all molecular orientations. The difference frequency is calculated by determining the difference chemical shift tensor with principal values ω_{ii}^{Δ} (i = 1, 2, 3). For axially symmetric tensors, the width of the difference tensor depends on the reorientation angle in a particularly simple way, $|\omega_{33}^{\Delta} - \omega_{11}^{\Delta}| = |3\,\delta \sin\beta_R|$.[31] Thus, for a given rigid-limit anisotropy, δ, the subcurves for various reorientation angles can be calculated, and the best fit to the experimental data yields the approximate amplitude of the motion, β_R. Information about the motional mechanism is then extracted by weighting the subcurves with the $R(\beta_R,t_m)$ specific to a motional model according to eq 2.

The main input parameters for the simulation were the principal values and orientation of the ^{15}N chemical shift tensor. The principal values were directly obtained from the ^{15}N powder spectrum of the protein and were σ_{11} = 60 ppm, σ_{22} = 80 ppm, and σ_{33} = 220 ppm. The anisotropy δ, defined as $\sigma_{33} - \sigma_{iso} = \sigma_{33} - (\sigma_{11} + \sigma_{22} + \sigma_{33})/3$, is thus 100 ppm, while the CSA span, $\sigma_{33} - \sigma_{11}$, is 160 ppm. The asymmetry parameter, $\eta = (\sigma_{22} - \sigma_{11})/\delta$, is 0.2. The ^{15}N powder spectrum not only provided the principal values but also allowed a suitable choice of Nt_r, since Nt_r should be approximately equal to $(\sigma_{33} - \sigma_{11})^{-1}$. The orientation of the ^{15}N chemical shift tensor is taken from model peptide studies: the σ_{33} axis lies in the peptide plane at an angle of about 20° from the N−H bond, and the σ_{11} axis is tilted by about −20° from the peptide plane.[22]

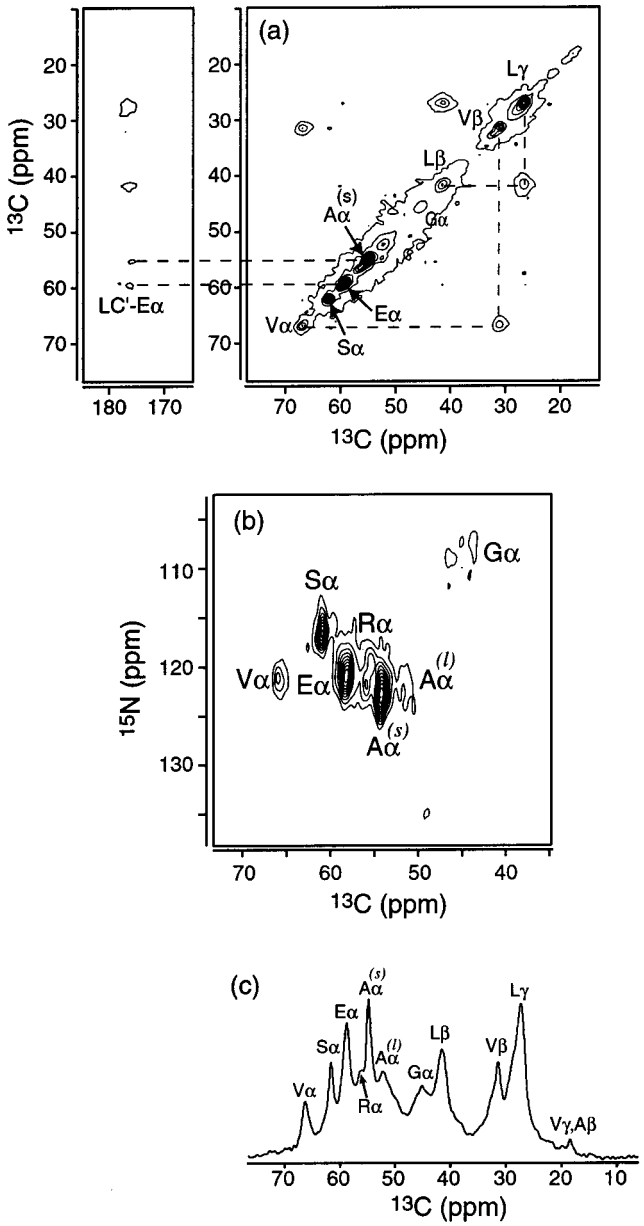

Figure 3. Resonance assignment of the TEASE-^{13}C, ^{15}N-labeled ACA hydrogel. (a) 2D ^{13}C−^{13}C correlation spectrum, acquired in 6 h. Dashed lines guide the eye for connectivities. (b) 2D ^{15}N−^{13}C correlation spectrum, acquired in 9 h. (c) 1D ^{13}C CP spectrum with summary of the ^{13}C assignment. Note the distinction between the liquid (l) and the solid (s) Ala peaks.

Results and Discussion

^{13}C Resonance Assignment. Before determining the mobilities of the various domains of the protein, we need to assign the ^{13}C spectra. The TEASE ^{13}C-labeling pattern yielded the following ^{13}C labels in the ACA protein: Ala (Cα), Gly (Cα), Val (Cα, Cβ), Leu (CO, Cβ, Cγ), and Ser (Cα). We used both ^{13}C−^{13}C and ^{15}N−^{13}C correlation experiments to obtain the assignment. The 2D ^{13}C−^{13}C correlation spectrum (Figure 3a) shows two distinct cross-peaks in the aliphatic region, which can be readily assigned to Val Cα/Cβ and Leu Cβ/Cγ on the basis of their characteristic chemical shifts. The assignment of Ser and Ala was less obvious due to the lack of connectivity patterns. The ^{15}N−^{13}C correlation spectrum (Figure 3b) alleviated this difficulty: the characteristic ^{15}N isotropic shift of Ser residues is about 116 ppm, while that of Ala is 122 ppm.[32] Thus, the resonance at 61 ppm was assigned to Ser Cα and the 54 ppm signal to Ala Cα. The Gly Cα peaks were identified by their unique upfield chemical shift at about 44 ppm. Multiple Gly peaks were observed in the ^{15}N−^{13}C spectrum, which is not surprising since Gly residues are present in all three domains of the protein with different conformations.

In addition to the ^{13}C signals expected from the TEASE labeling protocol, we also tentatively assigned Glu and Arg peaks. The Glu Cα peak (58.5 ppm) was identified on the basis of a carbonyl-Cα cross-peak in the 2D ^{13}C−^{13}C spectrum. This cross-peak was attributed to a Leu CO−Glu Cα connectivity, since there are eight Leu−Glu pairs in the protein sequence. The corresponding resonance in the ^{15}N−^{13}C spectrum shows a ^{15}N frequency of 119 ppm, which is consistent with the average Glu ^{15}N chemical shift of 120 ppm in proteins.[33] While in theory Glu Cα is not labeled by the TEASE protocol, the accidental lack of Gln in the minimal media likely caused partial Cα labeling of Gln and thus Glu, which is produced from Gln in a simple one-step reaction.[34] Due to the large number (32) of Glu residues in the protein, even a low level of scrambling could yield a nonnegligible signal in the spectra. The assignment of the 56 ppm peak to Arg Cα was chiefly based on the chemical shifts and the relative abundance of Arg residues (11) in the protein. The CODEX intensities of this peak were not analyzed subsequently. The assignment of the aliphatic ^{13}C signals is summarized in Figure 3c. Two Ala Cα signals, attributed to the rigid, solid fraction (55 ppm) and the mobile, liquid fraction (52 ppm), were separately identified and justified below.

Domain-Specific and Hydration-Dependent Fast Motions. The gelation model for the multidomain protein ACA postulates that the central domain is flexible and forms a random coil, while the terminal domains serve as intermolecular cross-linking agents.[5] If this model is correct, then the large-amplitude motion of the central domain should be reflected in the ^{13}C spectra. A reduced CP efficiency indicates large-amplitude motions with correlation times shorter than 10^{-5} s, the inverse of the ^{1}H−^{13}C dipolar coupling. Strong signals with narrow line widths in a direct-polarization (DP) spectrum also indicate segments that undergo fast large-amplitude motions. Thus, the rigid segments exhibit strong signals in the CP spectra, while the mobile residues show narrow and strong signals in the DP spectra.

Figure 4 displays the DP and CP ^{13}C spectra of 50% hydrated ACA. The DP spectrum (Figure 4a) is dominated by two signals, Ala Cα (52 ppm) and Gly Cα (44 ppm). Their line widths are about 55 Hz (0.75 ppm), which are significantly smaller than the average line widths of 160 Hz (2.1 ppm) in the CP spectrum. This suggests that part of the polypeptide chain is isotropically mobile. We assign these peaks to the Ala and Gly residues in the central domain, which contains a high percentage of all Gly (85%) and Ala (71%) residues in the protein. The large-amplitude motion of these residues is confirmed by the CP spectrum (Figure 4b), which shows drastically reduced intensities at these frequencies. In contrast, a number of other resonances have grown in intensity in the CP spectrum. The 55 ppm Cα peak can be assigned to Ala residues outside the central domain, in the terminal domains (8), and the linker regions (4). The presence of two Ala signals with

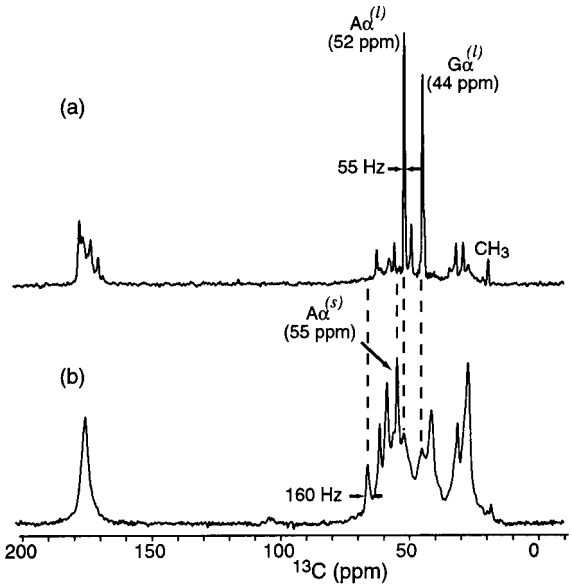

Figure 4. ^{13}C spectra of the multidomain protein hydrogel to determine domain-specific microsecond time scale dynamics. (a) ^{13}C direct-polarization spectrum. Sharp Gly (44 ppm) and Ala (52 ppm) Cα signals dominate the spectra. (b) ^{13}C cross-polarization spectrum. The Gly and 52-ppm Ala signals are suppressed due to mobility, while a number of other resonances have grown in intensities. Dashed lines guide the eye for peaks with different intensities between the two spectra. 25 mg of 50% hydrated protein was used.

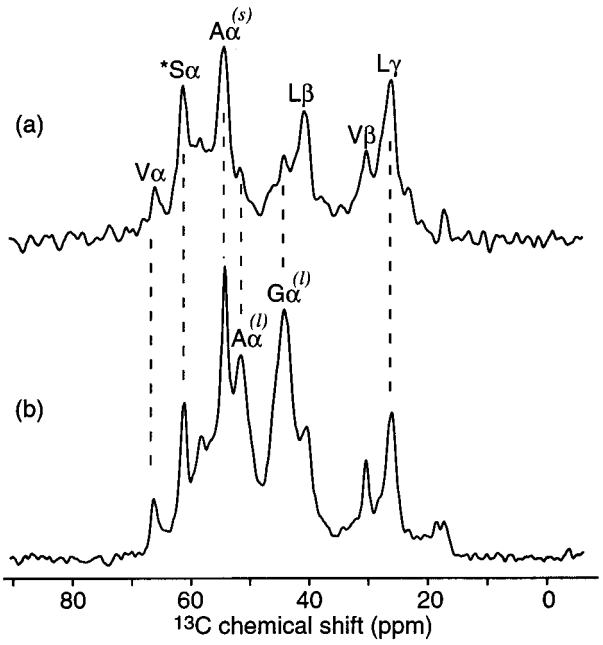

Figure 5. Hydration-dependent dynamics in the protein hydrogel. ^{13}C CP spectra for (a) 50% hydrated (1024 scans) and (b) 29% hydrated (2048 scans) samples show different intensity distributions. The 52 ppm Ala (l) Cα and 44 pm Gly (l) Cα signals were substantially reduced at the higher hydration level, indicating that the central domain swells and undergoes increased isotropic motion upon hydration. 6 mg of unlabeled protein was used.

different line widths and isotropic shifts indicates not only a mobility difference but also a conformational difference between the central domain and the rest of the protein: the average Ala Cα isotropic shift is about 51 ppm in random coils[32] and is shifted downfield by about 3 ppm in α-helices;[35] thus, the 55 ppm Cα signal strongly suggests that the Ala residues in the rigid parts of the protein are α-helical.

Unambiguous evidence that the helical parts of the protein correspond to the terminal domains is provided by the Val Cα resonance at 66 ppm. Compared to the random coil chemical shift of 61 ppm, this is a significant downfield displacement, which indicates that the Val resides are helical. Since all Val residues are located in the terminal domains (6) and the linker (2) regions and are excluded from the central domain, this Val Cα chemical shift shows that the terminal domains of the protein are helical. Consistently, the Cα isotropic shift of Ser residues, which are excluded from the central coil domain, is 62 ppm, which is clearly larger than the random coil value of 58 ppm.[33] Therefore, the engineered leucine-zipper sequence forms helical structures in the gel state.

The coexistence of an isotropically mobile domain and rigid domains in the protein hydrogel is further verified by the hydration dependence of the ^{13}C CP spectra. The spectral sensitivity of a 50% hydrated gel (Figure 5a) is substantially lower than that of a 29% hydrated gel (Figure 5b). This is consistent with the fact that in the wet sample a larger fraction of the protein becomes sufficiently mobile that cross-polarization is hindered. Interestingly, the intensity reduction upon increased hydration is not uniform across the spectra. Using the Ser Cα signal as a reference, we found that the 52 ppm Ala peak and the 45 ppm Gly peak decreased to 35% ± 2% upon hydration, while the 55 ppm Ala peak decreased to 66%. The different hydration dependence between the two Ala peaks supports the assignment of the downfield resonance to the rigid fraction of the protein and the upfield resonance to the mobile domain, which swells upon hydration. In comparison, the Val and Leu intensities are almost unchanged between the two spectra relative to Ser Cα. This means that the leucine-zipper domains, which contain most of the Val and Leu residues, are rigid on the microsecond time scale relevant to polarization transfer. It is noteworthy that the Leu side chain Cγ does not show reduced intensity with increasing hydration, as one might expect. This suggests that the Leu residues are tightly packed and well-ordered, which supports the notion that the helical domains form intermolecular aggregates in the gel network. In summary, the ^{13}C spectra provide strong evidence that the terminal domains of the protein form rigid helical structures with probable intermolecular aggregation, while the central domain is mobile and forms a random coil.

We note that it is not necessary to discriminate every individual residue in this triblock protein; rather, domain-specific assignment is the most important aspect. While individual residue resolution is not available in the ^{13}C spectra, most peaks are assigned domain specifically. For example, the Leu residues are solely located in the terminal domains of the protein, and the Ser and Val residues are excluded from the central coil domain. The solid Ala peak also excludes any contributions from the central domain. Moreover, if we make the reasonable assumption that the linker regions of the protein sequence are flexible, then their signals would be suppressed in the ^{13}C CP spectra and the CODEX spectra shown below. Without the linker signals, the Ser Cα, the 55 ppm Ala Cα, and Val Cα signals all reflect the properties of the terminal domains exclusively.

Slow Motions in the Leucine-Zipper Domains. While the leucine-zipper domains are rigid on the

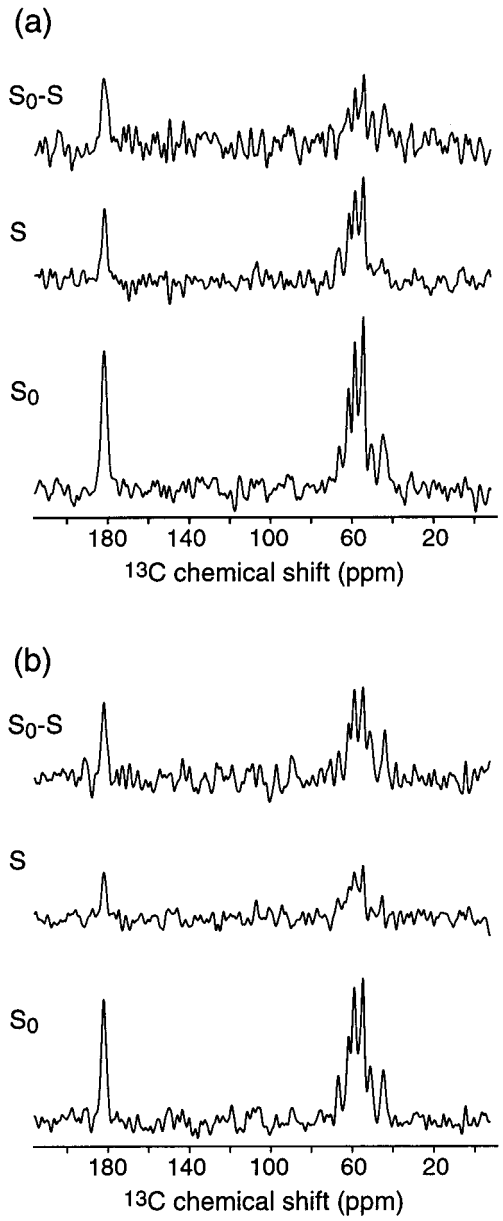

Figure 6. Representative ^{13}C-detected ^{15}N-CODEX spectra of the protein hydrogel: (a) reference (S_0), exchange (S), and difference ($S_0 - S$) spectra at $t_m = 50$ ms; (b) reference (S_0), exchange (S), and difference ($S_0 - S$) spectra at $t_m = 500$ ms. Except for the difference spectra, each spectrum was acquired with 8192 scans at 293 K at a spinning speed of 5.5 kHz. $Nt_r = 727$ μs.

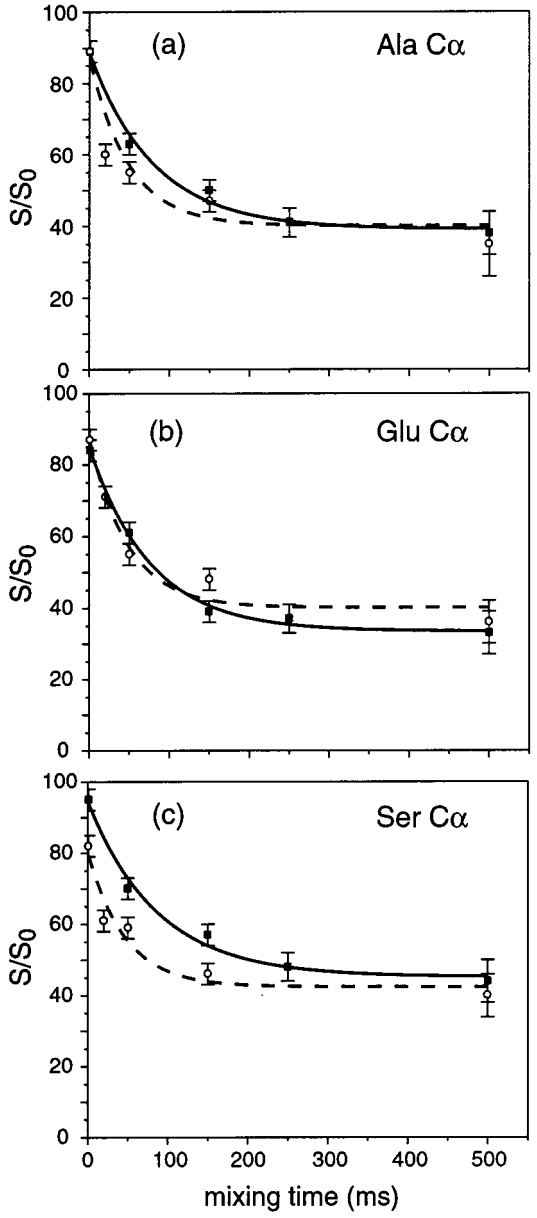

Figure 7. Mixing-time (t_m) dependence of the CODEX exchange intensity S/S_0 for various sites: (a) Ala Cα (55 ppm); (b) Glu Cα; (c) Ser Cα. Squares and circles represent data acquired at 293 and 308 K, respectively. Solid and dashed lines are the respective best fits.

microsecond time scale, they are mobile on the millisecond time scale, as manifested in the CODEX experiment. Figure 6 shows the ^{13}C-detected ^{15}N CODEX spectra of ACA for mixing times of 50 ms (a) and 500 ms (b), acquired with ^{15}N CSA recoupling time of $Nt_r = 727$ μs. The reference spectra (S_0) at the two mixing times are nearly identical due to the long ^{15}N T_1 relaxation time (7 s). The exchange spectra (S) show clearly reduced intensities compared to those of the reference spectra, indicating that the ^{15}N chemical shift tensors have reoriented during t_m. This reflects reorientations of molecular segments within as little as 50 ms. The difference in intensities increased with the mixing time. Because of ^{1}H−^{15}N cross-polarization, only the rigid fraction of the protein was detected in the spectra, while the signals of the mobile residues were suppressed. Note that only the ^{13}Cα and ^{13}CO signals were detected, since these are directly bonded to the amide ^{15}N and were selected by the ^{15}N−^{13}C TEDOR sequence.

The normalized CODEX intensities, S/S_0, were plotted as a function of t_m in Figure 7 for three resolved Cα signals, Ala (55 ppm), Glu, and Ser. Among these three peaks, the Ala solid fraction peak and the Ser peak have no contributions from the central coil domain, while the Glu peak results mainly from the helical domains but also contain small contributions from the coil domain. Altogether, spectra with five different mixing times were recorded. Remarkably, the intensity decays for all three peaks were well fit by single-exponential functions with similar decay constants: 80 ± 8 ms for Ala, 76 ± 8 ms for Glu, and 86 ± 19 ms for Ser. The average decay constant is 81 ± 12 ms. Equilibrium values of the three curves are also similar, at 0.39 ± 0.06. Correlation times of 75−85 ms are consistent with DWS measurements,

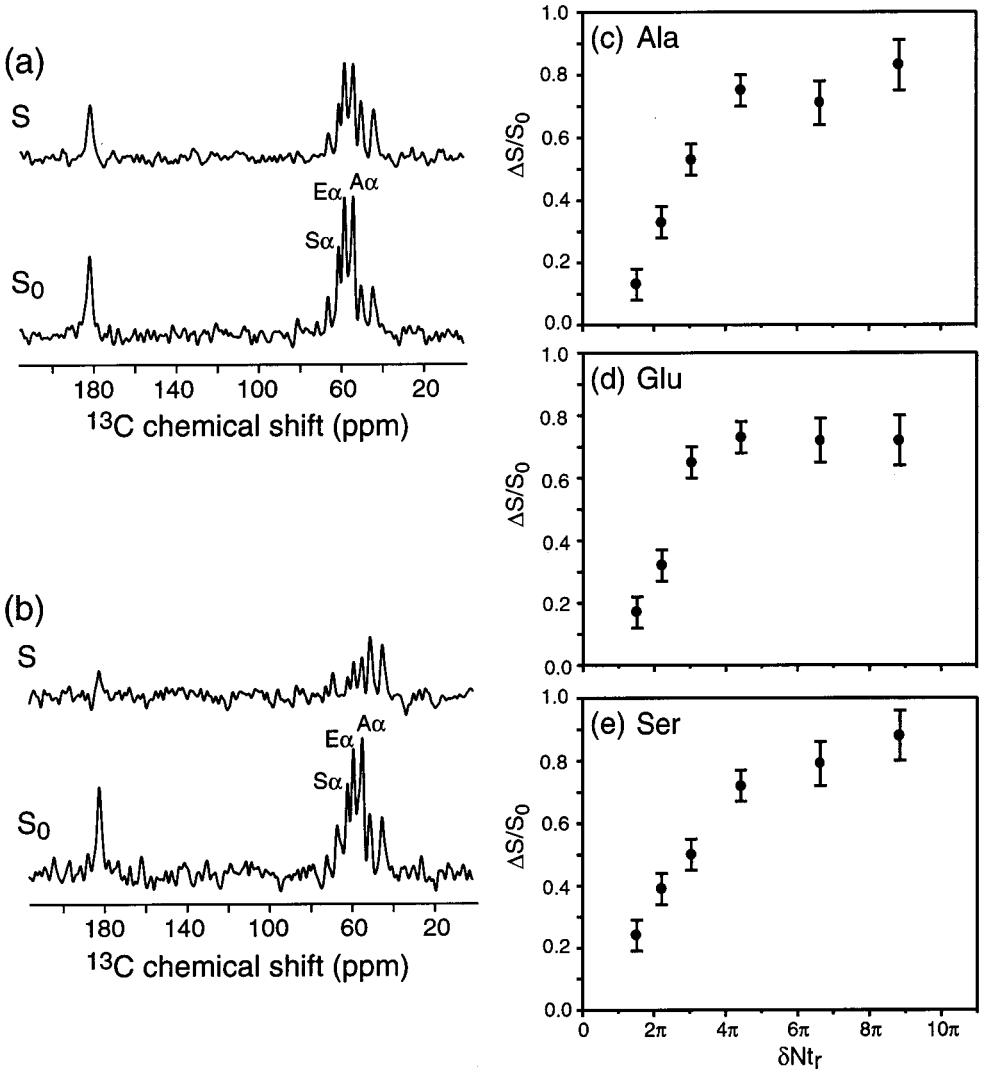

Figure 8. Excitation-time (Nt_r) dependence of the exchange intensities. (a) CODEX reference (S_0) and exchange (S) spectra for $N = 2$ ($Nt_r = 363.6$ μs). (b) CODEX reference (S_0) and exchange (S) spectra for $N = 6$ ($Nt_r = 1.09$ ms). The normalized pure-exchange intensities $\Delta S/S_0$ as a function of δNt_r are shown for Ala Cα (c), Glu Cα (d), and Ser Cα (e). The mixing time was 250 ms. An experimental ^{15}N CSA of $\delta = 2\pi \times 3.04$ kHz was used to calculate δNt_r.

which suggest cooperative network junction mobility on time scales of hundreds of milliseconds to tens of seconds.[5]

To gain more insight into the nature of the leucine-zipper motions, we examined the temperature dependence of the exchange. At 308 K, the normalized exchange intensities (Figure 7, open circles) yielded substantially shorter correlation times: 28 ± 16 ms for Ala, 48 ± 16 ms for Glu, and 46 ± 22 ms for Ser. The reduced motional correlation times at the elevated temperature indicate that the leucine-zipper motion is thermally activated. The less than 100% intensity at small t_m probably resulted from the very short mixing time, 0.2 ms, used for the reference experiment. At this short mixing time, the transverse ^{15}N magnetization may not have completely dephased, thus biasing the reference intensity S_0 to larger values.

The mixing-time-dependent CODEX intensities decay to about 40%. This incomplete exchange can be partly attributed to the ^{15}N CSA recoupling time (727 μs) used in the experiments. This recoupling time corresponded to $\delta Nt_r = 2\pi \times 3.04$ kHz $\times$ 727 μs $= 4.4\pi$, which is shorter than the $\delta Nt_r \geq 7\pi$ required to achieve nearly complete exchange, as we show below (Figure 9).

Amplitude and Mechanism of Slow Motion. The uniformity of the motional correlation times for different residues extracted from the mixing-time dependence of the CODEX data strongly suggests that each helical domain of the polypeptide chains moves as a rigid body. To obtain information on the amplitude and geometry of this slow motion, we investigated the Nt_r dependence of the exchange. Figure 8 shows the CODEX spectra for $N = 2$ and 6, acquired with a mixing time of 250 ms, which was essentially in the full-exchange limit. From these spectra, the Nt_r-dependent pureexchange intensities $E(t_m,\delta Nt_r) = \{\Delta S\}/\{S_0\}$ were plotted for Ala, Glu, and Ser (Figure 8c−e). In the following, we extract the motional amplitudes and consider several motional models to interpret this CODEX Nt_r dependence.

I. Motional Amplitude. Model-independent information on the amplitude of the leucine-zipper motion is obtained by simulating the Nt_r-dependent pure-exchange subcurves $\epsilon(\alpha_R,\beta_R,\gamma_R,\delta Nt_r)$ for various reorientation angles β_R. Since the ^{15}N chemical shift tensor in peptides is only slightly nonuniaxial, the influence of the α_R and γ_R reorientation angles on the simulation is small and is thus neglected here. Figure 9 shows the simulated β_R-dependent CODEX curves,

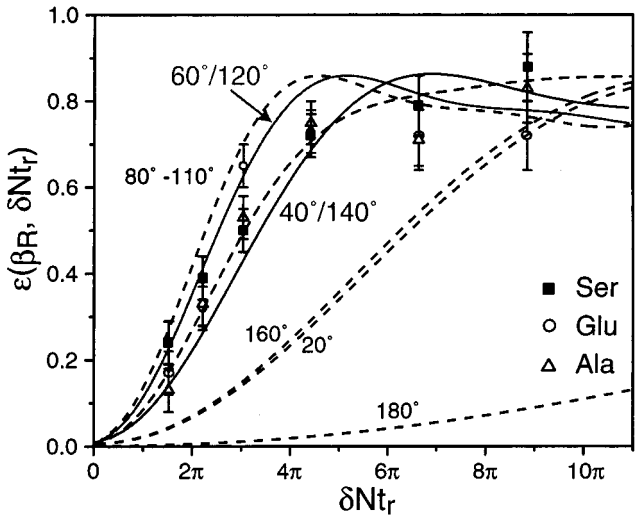

Figure 9. Simulated Nt_r-dependent pure-exchange curves $\epsilon(\beta_R,\delta Nt_r)$ for various reorientation angles β_R, superimposed with the experimental data. The simulated curves were scaled to 77% to reflect the incomplete exchange of the experimental intensities. A ^{15}N CSA of $\delta = 100$ ppm was used. The experimental data fall between $\beta_R = 60°$ and $\beta_R = 40°$.

scaled to 77%, to reflect the fact that the experimental intensities at long CSA excitation times do not reach full exchange (see below). It can be seen that after scaling the simulated exchange subcurves for $\beta = 40°$ and $\beta = 60°$ encompass the intensities for the three representative residues reasonably well. This indicates that the average helix reorientation angle is approximately 50°.

II. Uniaxial Rotational Diffusion. To analyze the experimental Nt_r-dependent exchange intensities more quantitatively, we first consider the model of uniaxial rotational diffusion of the leucine zippers around the helical axis.[12] Rigid-body rotations of helices have been detected for naturally occurring proteins such as rhodopsin and potassium channel proteins.[36−38] A rigid-body rotation of the leucine-zipper domains would be consistent with the observed similarity of the motional rates and equilibrium values for different residues.

In the uniaxial rotational diffusion model, the molecular reorientations are more conveniently expressed in terms of the rotation angle, ψ, rather than the reorientation angle, β_R. The rotation angle is the angle between the tensor axes before and after the motion, projected onto a plane normal to the motional axis (Figure 10a). It is related to the reorientation angle according to

$$\cos\beta_R = \cos^2\beta_{PM} + \sin^2\beta_{PM}\cos\psi \qquad (4)$$

where β_{PM} is the angle between the main chemical shift axis and the rotational axis.[22] Since the helical axis is approximately parallel to the N−H bond, and the main ^{15}N chemical shift tensor axis is σ_{33}, the rotation around the helical axis is equivalent to the precession of the ^{15}N σ_{33} axis on a cone around the N−H bond. We assume a Gaussian distribution of the rotation angle ψ with a single-sided width of $\sigma = \sqrt{2t_m/\tau_c}$. The resulting $R(\psi,t_m)$ for different t_m/τ_c values are shown in Figure 10b. The curve for $t_m/\tau_c = 3.1$ is relevant under our experimental conditions, since $t_m = 250$ ms was used in the Nt_r dependence measurements and the motional correlation times were found to be about 80 ms from the mixing-time dependence experiments.

Figure 10c shows the CODEX subcurves $\epsilon(\psi,\delta Nt_r)$ for various rotation angles ψ and assuming a cone semi-angle of 30°. Weighting these with the rotation-angle distribution, $R(\psi,t_m)$, we obtained the Nt_r-dependent pure-exchange curves $E(t_m,\delta Nt_r)$ for various t_m values (Figure 10d). All curves show positive slopes, corresponding to the fact that small-amplitude motions make increasing contributions to the exchange intensities with increasing Nt_r. At larger t_m/τ_c values, the initial slopes of the curves become steeper. At t_m/τ_c greater than 5.0, the difference among the curves becomes minor, indicating that the full exchange limit has been reached. At $t_m/\tau_c = 3.1$, the CODEX curve rises rapidly until $\delta Nt_r \approx 5\pi$ and then levels off to a final value of 1. The simulation for $t_m/\tau_c = 3.1$ fits the experimental intensities of the three resolved Cα peaks quite well (Figure 10d), suggesting that the uniaxial rotational diffusion model describes the motion of the leucine-zipper domains adequately.

The angle $\beta_{PM} = 30°$ used in the simulations deviates from the value of 17−20° between the N−H bond and the σ_{33} axis of the ^{15}N chemical shift tensor. This deviation may result from the fact that the N−H bonds are tilted from the axis of an ideal α-helix by about 10°, so that the use of the N−H bond as the rotation axis is only approximate. In addition, we do not attempt to distinguish between the axis of an individual helix and of the helical bundle, which can differ by about 20°.[39,40]

III. Isotropic Rotational Diffusion. Next, we consider the isotropic rotational diffusion model. Since the protein hydrogel contains a highly flexible central domain, an isotropic motion of the attached leucine zippers is possible. The reorientation angle distribution, $R(\beta_R,t_m)$, for isotropic rotational diffusion of an axially symmetric tensor can be obtained by using the rotational diffusion equation.[12,41] In the limit of $t_m/\tau_c = \infty$, the reorientation angle distribution is simply $R(\beta_R,t_m) = \sin\beta_R$ (Figure 11a). The use of only β_R rather than all three Euler angles, α_R, β_R, and γ_R, is a fair approximation for the amide ^{15}N chemical shift tensor, since its asymmetry is low, $\eta \approx 0.2$. The Nt_r-dependent CODEX curves for isotropic rotational diffusion are shown in Figure 11b. The initial slopes and equilibrium values of the curves are clearly larger than those for uniaxial rotational diffusion. This reflects the strong contribution of large reorientation angles due to the sin β_R weighting function. The curve for $t_m/\tau_c = 3.1$ (Figure 11c) deviates significantly from the experimental data, indicating that the isotropic rotational diffusion model does not adequately describe the leucine-zipper motion.

IV. Random Jump. The last motional model to be considered is the random jump motion, in which the reorientation angle distribution is a single peak at $\beta_R = 0$ and a broad sin β_R contribution. Since the non-reorienting segments do not contribute to the Nt_r-dependent CODEX curves, $E(t_m,\delta Nt_r)$ for this model is equal to the isotropic rotational diffusion in the asymptotic limit scaled by the fraction of reorienting segments. We found that the simulated curve for random jumps with 80% of all sites undergoing exchange (Figure 11c, dashed line) fits the experimental data quite well. In other words, a random jump motion in which 20% of the leucine-zipper domains remain at, or return to, their initial orientations also describes the experimental data adequately.

Proposed Leucine-Zipper Motion and Its Significance. Our simulations show that either uniaxial

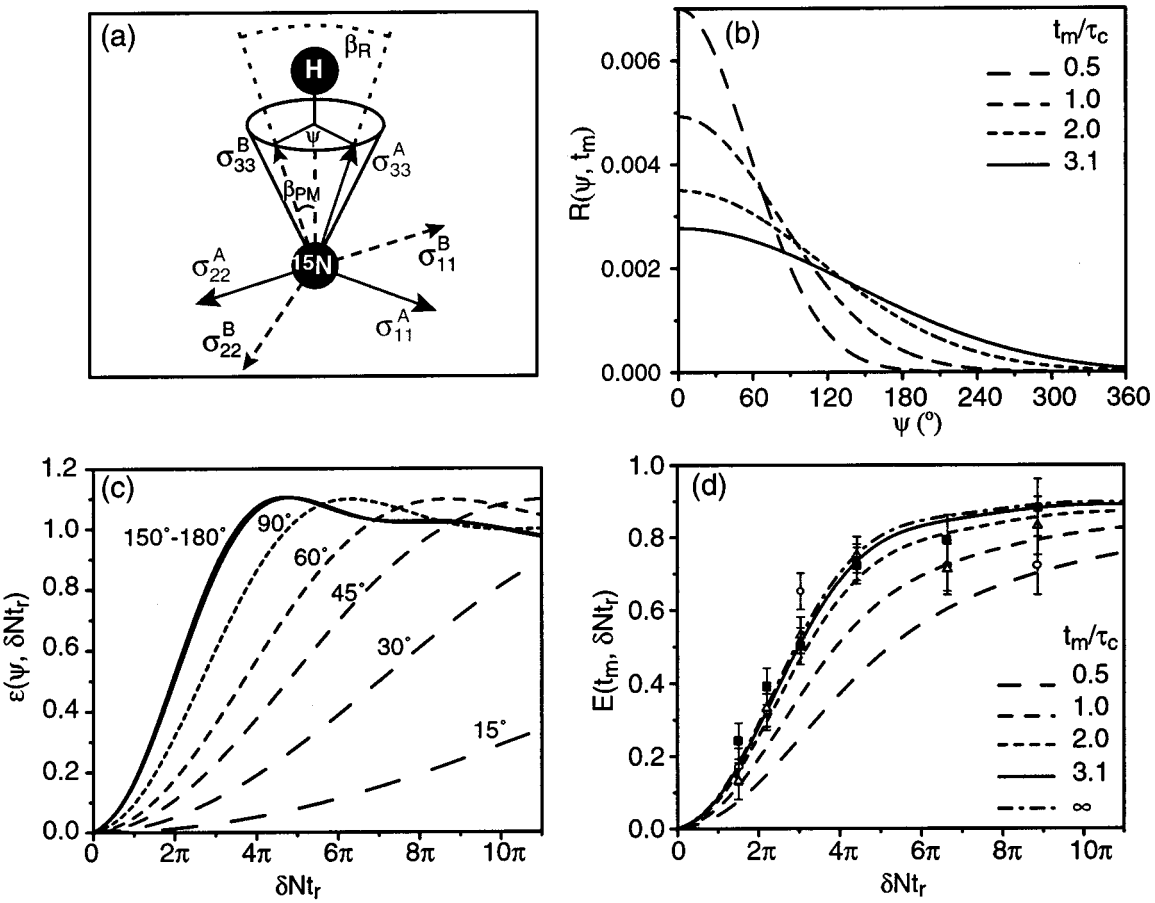

Figure 10. Simulated Nt_r-dependent CODEX curves for the uniaxial rotational diffusion model. (a) In the uniaxial rotational diffusion model, the rotation angle ψ and the reorientation angle β_R are related through the cone semiangle β_{PM}. The principal axis systems before (A) and after (B) the reorientation are illustrated. The angle between the N−H bond and the σ_{33} axis defines β_{PM}. (b) Rotation-angle distribution $R(\psi,t_m)$ for a Gaussian function with varying widths t_m/τ_c. (c) Nt_r-dependent CODEX subcurves $\epsilon(\psi,\delta Nt_r)$ for rotation angles ψ = 15°, 30°, 45°, 60°, 90°, and 150°−180°. A cone semiangle β_{PM} = 30° and t_m = 250 ms were used in the simulations. (d) Simulated Nt_r-dependent CODEX curves $E(t_m,\delta Nt_r)$ for varying t_m/τ_c values, superimposed with the experimental data for Ser (squares), Glu (circles), and Ala (triangles).

rotational diffusion or a random jump motion with about 20% nonexchanging component fit the experimental data. Identifying the correct motional model requires further experimentation and comparison between NMR data and fluorescence exchange data. We hypothesize that the motion observed in CODEX experiments correlates with strand exchange between helical bundles. Our hypothesis is based on previously reported strand exchange data indicating individual helices dissociate and associate via a two-step mechanism.[42,43] One step is independent of concentration, which suggests equilibrium exists between a superhelical aggregated state and an aggregated transition state. The other step depends on concentration, which suggests equilibrium between the aggregated transition state and a final state that can be either a free helix or another, smaller helical bundle.

Comparing a series of concentration-dependent NMR experiments with a series of concentration-dependent fluorescence experiments could identify the nature of motion observed by the CODEX experiment. The uniaxial rotational diffusion model would be consistent with a physical picture of helical aggregation where one or a small number of helices maintain their helix axis orientation but undergo a transverse motion as they rotate within the superhelical aggregate. In this case, either a series of correlated uniaxial rotations or a single uniaxial rotation serves as the mechanism of motion between the superhelical state and the aggregated transition state. As such, the time scale of motion measured by the CODEX experiment would not depend on concentration. This model could be further validated if the time scale of motion measured by CODEX correlates with the characteristic time between the superhelical state and the aggregated transition state as measured by fluorescence exchange.

On the other hand, the random jump model would be consistent with a physical picture where helices dissociate from their existing bundles by random reorientations and associate with other bundles whose orientations are uncorrelated with the previous bundles. A good fit to the data requires that about 20% of the helices retain their original orientation. This could result either from helices that never dissociated or from helices that dissociated but subsequently return to their original bundle. The hypothesis of a nonexchanging fraction could be tested by applying the CODEX sequence twice to observe the dynamics of the mobile sites that have already been selected by CODEX.[31] In this random jump model, the time scale of motion measured by the CODEX experiment would depend on concentration. This model could be further validated if the time scale of motion measured by CODEX correlates with the characteristic times between all three states as measured by fluorescence exchange.

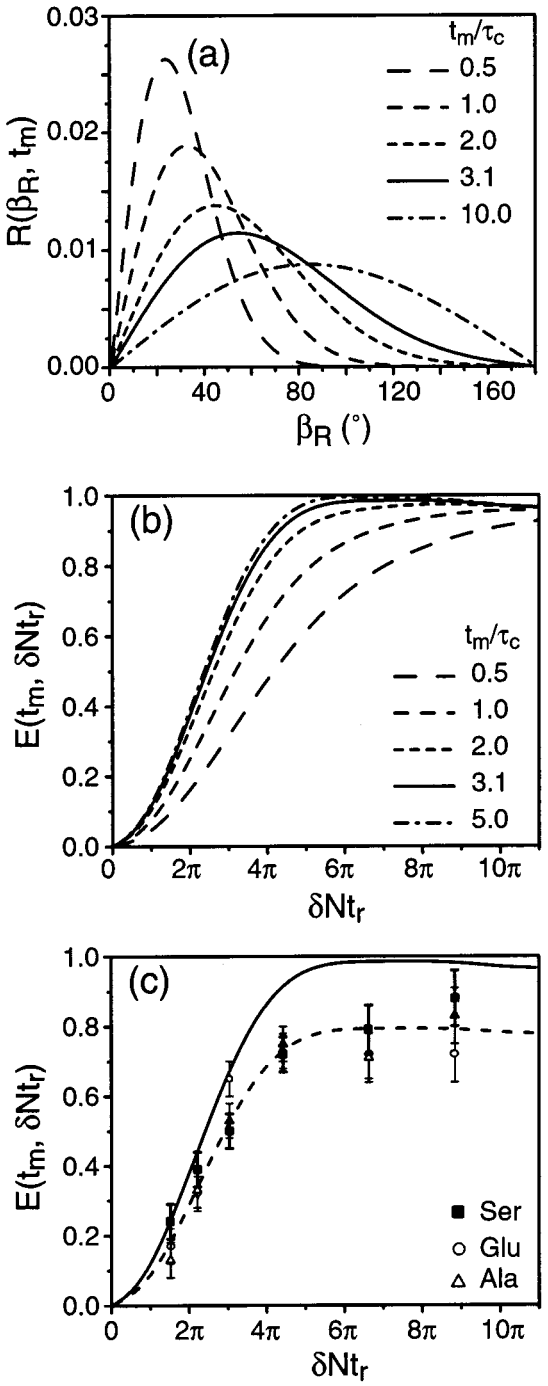

Figure 11. Simulated Nt_r-dependent CODEX curves for the isotropic rotational diffusion model and the random jump model. (a) Reorientation-angle distribution $R(\beta_R,t_m)$ for varying t_m/τ_c values. (b) Nt_r-dependent CODEX curves $E(t_m,\delta Nt_r)$ for varying t_m/τ_c values. (c) Simulated Nt_r dependence curve for $t_m/\tau_c = 3.1$ for the isotropic rotational diffusion (solid line) and for a random jump motion with 20% nonexchanging component (dashed line). The experimental data are the same as in Figure 10.

The current investigation of the amplitude and mechanism of slow motions of the leucine-zipper domains relies on the knowledge of the magnitude and orientation of the ^{15}N chemical shift tensor. While the CSA value we use for simulating the ^{15}N exchange (CSA span = 160 ppm or δ = 100 ppm) is consistent with the average ^{15}N CSAs of model peptides and proteins, small variations in the ^{15}N tensor orientation and magnitude have been measured by solution NMR.[44,45] The approximations of the ^{15}N chemical shift tensor and the sensitivity of the spectra limit the precision of the extracted reorientation angles. Further information about the motional geometry of the leucine zippers and further distinction between the random jump model and the uniaxial rotational diffusion model could be obtained using other spin interactions such as the carbonyl chemical shift tensor with different orientations in the molecular segments. The detailed dynamics information that can be potentially extracted from the CODEX experiment makes this a promising tool for investigating millisecond time scale dynamics in proteins in general.

Conclusion

We have used ^{13}C and ^{15}N magic-angle spinning solid-state NMR spectroscopy to investigate the dynamic and structural properties of a multidomain protein hydrogel, which contains two leucine-zipper domains flanking a central polyelectrolyte domain. The ^{13}C NMR spectra confirm the hypothesis that the central domain is isotropically mobile, while the terminal leucine-zipper domains are more rigid. These dynamic differences exist on time scales much shorter than 10^{-5} s, dictated by the ^{13}C−^{1}H dipolar couplings that underlie the differences between cross-polarization and direct polarization experiments. The preferential suppression of the Ala and Gly Cα intensities with increasing hydration confirms the hypothesis that the central domain is flexible and swells upon hydration. From a structural point of view, the ^{13}Cα isotropic shifts of the residues exclusively located in the terminal domains of the protein sequence (e.g., Val) indicate that these domains are helical, while the chemical shifts of the mobile Ala component supports the random coil conformation for the central domain. Therefore, the ^{13}C NMR spectra directly confirm the architectural design of the polypeptide sequence and the essential features of the gelation model.

The multidomain protein hydrogel ACA not only is dynamic on the sub-microsecond time scale but also moves on the millisecond time scale. The CODEX experiments show that the leucine-zipper domains undergo thermally activated, rigid-body reorientations with a correlation time of about 80 ms at room temperature and with an average reorientation angle of about 50°. Two models, uniaxial rotational diffusion and random jump motions, reproduce the experimental data. Both models can explain a dynamic gel structure where leucine-zipper aggregates act as continuously exchanging physical cross-links. Further NMR experiments exploring concentration dependence and different nuclear spin interactions are necessary to identify the exact model for dynamics in the protein hydrogel.

Acknowledgment. This work was partially supported by the NSF Materials Science and Engineering Center at the University of Massachusetts, Amherst. M. Hong acknowledges NSF for a POWRE award and the Beckman Foundation for a Young Investigator Award. E. R. deAzevedo thanks the FAPESP-Brazil program for a graduate fellowship.

References and Notes

(1) Hubbell, J. A. *Biotechnology* **1995**, *13*, 565.
(2) Langer, R. *Science* **1990**, *249*, 1527.
(3) Bell, C. L.; Peppas, N. A. *Biomaterials* **1996**, *17*, 1203.
(4) Hill-West, J. L.; Chowdhury, S. M.; Slepian, M. J.; Hubbell, J. A. *Proc. Natl. Acad. Sci. U.S.A.* **1994**, *91*, 5967.

(5) Petka, W. A.; Harden, J. L.; McGrath, K. P.; Wirtz, D.; Tirrell, D. A. *Science* **1998**, *281*, 389.
(6) Rehage, G. *Kunstoffe* **1963**, *53*, 605.
(7) Nijenhuis, K. T. *Colloid Polym. Sci.* **1981**, *259*, 522.
(8) Morris, E. R.; Rees, D. A.; Robinson, C. *J. Mol. Biol.* **1980**, *138*, 349.
(9) O'Shea, E. K.; Klemm, J. D.; Kim, P. S.; Alber, T. *Science* **1991**, *254*, 539.
(10) Harbury, P. B.; Zhang, T.; Kim, P. S.; Alber, T. *Science* **1993**, *262*, 1401.
(11) Lumb, K. J.; Kim, P. S. *Science* **1995**, *268*, 436438.
(12) Schmidt-Rohr, K.; Spiess, H. W. *Multidimensional Solid-State NMR and Polymers*, 1st ed.; Academic Press: San Diego, 1994; p 478.
(13) Griffin, R. G. *Nat. Struct. Biol.* **1998**, *NMR Suppl.*, 508.
(14) Hong, M. *J. Magn. Reson.* **1999**, *139*, 389.
(15) Hong, M.; Jakes, K. *J. Biomol. NMR* **1999**, *14*, 71.
(16) Bennett, A. E.; Rienstra, C. M.; Auger, M.; Lakshmi, K. V.; Griffin, R. G. *J. Chem. Phys.* **1995**, *103*, 6951.
(17) Hong, M.; Griffin, R. G. *J. Am. Chem. Soc.* **1998**, *120*, 7113.
(18) Gullion, T.; Schaefer, J. *J. Magn. Reson.* **1989**, *81*, 196.
(19) States, D. J.; Haberkorn, R. A.; Ruben, D. J. *J. Magn. Reson.* **1982**, *48*, 286.
(20) deAzevedo, E. R.; Kennedy, S. B.; Hong, M. *Chem. Phys. Lett.* **2000**, *321*, 43.
(21) deAzevedo, E. R.; Bonagamba, T. J.; Hu, W.; Schmidt-Rohr, K. *J. Am. Chem. Soc.* **1999**, *121*, 8411.
(22) Oas, T. G.; Hartzell, C. J.; Dahlquist, F. W.; Drobny, G. P. *J. Am. Chem. Soc.* **1987**, *109*, 5962.
(23) Mai, W.; Hu, W.; Wang, C.; Cross, T. A. *Protein Sci.* **1993**, *2*, 532.
(24) Wu, C. H.; Ramamoorthy, A.; Gierasch, L. M.; Opella, S. J. *J. Am. Chem. Soc.* **1995**, *117*, 6148.
(25) Harbison, G.; Herzfeld, J.; Griffin, R. G. *J. Am. Chem. Soc.* **1981**, *103*, 4752.
(26) Lee, D.-K.; Ramamoorthy, A. *J. Magn. Reson.* **1998**, *133*, 204.
(27) Shoji, A.; Ando, S.; Kuroki, S.; Ando, I.; Webb, G. A. *Annu. Rep. NMR Spectrosc.* **1993**, *26*, 55.
(28) Hing, A. W.; Vega, S.; Schaefer, J. *J. Magn. Reson.* **1992**, *96*, 205.
(29) Hong, M. *J. Biomol. NMR* **1999**, *15*, 1.
(30) Pines, A.; Gibby, M. G.; Waugh, J. S. *J. Chem. Phys.* **1973**, *59*, 569.
(31) deAzevedo, E. R.; Bonagamba, T. J.; Hu, W.; Schmidt-Rohr, K. *J. Chem. Phys.* **2000**, *112*, 8988.
(32) Wuthrich, K. *NMR of Proteins and Nucleic Acids;* John Wiley: New York, 1986
(33) Wishart, D. S.; Sykes, B. D.; Richards, F. M. *J. Mol. Biol.* **1991**, *222*, 311.
(34) Lehninger, A. L.; Nelson, D. L.; Cox, M. M. *Principles of Biochemistry*, 2nd ed.; Worth Publishers: New York, 1993; p 1013.
(35) Spera, S.; Bax, A. *J. Am. Chem. Soc.* **1991**, *113*, 5490.
(36) Farrens, D. L.; Altenbach, C.; Yang, K.; Hubbell, W. L.; Khorana, H. G. *Science* **1996**, *274*, 768.
(37) Perozo, E.; Cortes, D. M.; Cuello, L. G. *Science* **1999**, *285*, 73.
(38) Cha, A.; Snyder, G. E.; Selvin, P. R.; Bezanilla, F. *Nature* **1999**, *402*, 809.
(39) Lovejoy, B.; Choe, S.; Cascio, D.; McRorie, D. K.; DeGrado, W. F.; Eisenberg, D. *Science* **1993**, *259*, 1288.
(40) Harbury, P. B.; Kim, P. S.; Alber, T. *Nature* **1994**, *371*, 80.
(41) Wefing, S.; Kaufmann, S.; Spiess, H. W. *J. Chem. Phys.* **1988**, *89*, 1234.
(42) Wendt, H.; Baici, A.; Bosshard, H. R. *J. Am. Chem. Soc.* **1994**, *116*, 6973.
(43) Wendt, H.; Berger, C.; Baici, A.; Thomas, R. M.; Bosshard, H. R. *Biochemistry* **1995**, *34*, 4097.
(44) Fushman, D.; Cowburn, D. *J. Biomol. NMR* **1999**, *13*, 139.
(45) Fushman, D.; Cowburn, D. *J. Am. Chem. Soc.* **1998**, *120*, 7109.

MA010768J